Book Chapter

Optimizing Carrier Frequency for Implantable Human Body Communication System through Trade-off Between Transmission Efficiency and Electromagnetic Interference

Miyu Kodama and Dairoku Muramatsu*

The University of Electro-Communications 1-5-1 Chofugaoka, Chofu, Tokyo 182-8585, Japan

***Corresponding Author:** Dairoku Muramatsu, The University of Electro-Communications 1-5-1 Chofugaoka, Chofu, Tokyo 182-8585, Japan

Published **December 19, 2024**

This Book Chapter is a republication of an article published by Miyu Kodama and Dairoku Muramatsu at AIP Advances in July 2024. (Miyu Kodama, Dairoku Muramatsu; Determining carrier frequency for implantable human body communication based on transmission efficiency–electromagnetic interference trade-off. AIP Advances 1 July 2024; 14 (7): 075208. https://doi.org/10.1063/5.0210654)

How to cite this book chapter: Miyu Kodama, Dairoku Muramatsu. Optimizing Carrier Frequency for Implantable Human Body Communication System through Trade-off Between Transmission Efficiency and Electromagnetic Interference. In: Valentin-Adrian Niță, editor. Prime Archives in Sensors: 3rd Edition. Hyderabad, India: Vide Leaf. 2024.

© The Author(s) 2024. This article is distributed under the terms of the Creative Commons Attribution 4.0 International License (http://creativecommons.org/licenses/by/4.0/), which permits

unrestricted use, distribution, and reproduction in any medium, provided the original work is properly cited.

Acknowledgments: A part of this research was funded by JSPS KAKENHI Grant No. JP22H03996, KDDI Foundation, and Azbil Yamatake General Foundation.

Conflict of Interest: The authors have no conflicts to disclose.

Author Contributions: Miyu Kodama: Conceptualization (supporting); Data curation (equal); Formal analysis (equal); Funding acquisition (supporting); Investigation (lead); Methodology (supporting); Validation (equal); Visualization (equal); Writing – original draft (lead); Writing – review & editing (supporting). **Dairoku Muramatsu**: Conceptualization (lead); Data curation (equal); Formal analysis (equal); Funding acquisition (lead); Investigation (supporting); Methodology (lead); Project administration (lead); Resources (lead); Software (lead); Supervision (lead); Validation (equal); Visualization (equal); Writing – original draft (supporting); Writing – review & editing (lead).

Data Availability: The data that support the findings of this study are available from the corresponding author upon reasonable request.

Abstract

This study proposes a novel methodology for optimizing the optimal carrier frequency for implantable human body communication (HBC) by focusing on the trade-off between transmission efficiency and electromagnetic interference (EMI) robustness. Traditional radio communication technologies use high-frequency bands, which pose some challenges, such as increased power consumption, EMI with other devices, and security risks. Implantable HBC is a promising alternative, wherein the human body is used as a transmission medium. Through phantom experiments simulating the human abdomen, we assess the transmission characteristics of implantable HBC between an abdominal neurostimulator and an external controller

across a frequency range of 1–100 MHz. Results revealed that maximum transmission gain was achieved at 37.2 MHz. Moreover, rapid signal attenuation occurred beyond a minimal distance from the skin, indicating enhanced communication efficiency, reduced EMI, and enhanced information security. An evaluation index (*EI*) was also proposed to quantitatively assess the balance between transmission efficiency and EMI and optimize an appropriate carrier frequency for specific implantable HBC applications. This study advances the field of implantable medical devices by optimizing communication performance while addressing key challenges in EMI and security.

Keywords

Wearable Technology; Electromagnetic Interference; Antennas; Electromagnetic Compatibility; Wireless Communications; Telecommunications Engineering; Bioelectromagnetics; Biomedical Engineering; Biomedical Equipment; Tissue Structure

Introduction

Implantable medical devices (IMDs) are commonly used in modern medicine to improve diagnosis and quality of life. IMDs, such as pacemakers and capsule endoscopes, exchange sensor and control information with external devices via wireless communication [1–4]. The majority of these IMDs operate within the 400-MHz band assigned for 400-MHz Medical Device Radiocommunications Service (MedRadio) and Medical Implant Communication Service (MICS) band or the 2.45-GHz Industrial Scientific and Medical (ISM) band to establish wireless communication with external devices [5–8]. However, these high-frequency bands suffer from increased power consumption due to signal loss in biological tissues [9–14], electromagnetic interference (EMI) with other electrical devices [15–20], and security risks for unauthorized wireless access [21–25]. To address these issues, implantable human body communication (HBC) is proposed herein, wherein the human body is used as a transmission path for electrical signals with frequencies of several tens of MHz.26 HBC enables low-power, low-noise

communications because the electric field is distributed only in the vicinity of the human body via a quasi-static electric field around the human body.27 Previous studies have recommended the use of the 13.56-MHz band of ISM and the 21-MHz band of IEEE 802.15.6 as carrier frequencies for HBC in a wearable environment.28–30 However, the optimal carrier frequency for implantable HBC has not yet been identified [31,32]. This study focused on implantable HBC for communicating between an abdominal implantable medical device such as a neurostimulator and its controller on the skin surface. A method for optimizing the optimal carrier frequency for implantable HBC based on the trade-off between transmission efficiency and EMI robustness was proposed by conducting phantom experiments.

Measurement Setup

Figure 1 shows the measurement setup for evaluating the transmission characteristics of implantable HBC between the inside and outside of the abdomen. In the experiment, the human abdomen was mimicked using three phantoms with the electrical properties of the skin, fat, and muscle. Transmitter (TX) electrodes were placed inside the phantom, and receiver (RX) electrodes were placed on the phantom's skin layer. Table 1 summarizes the phantom's information in terms of dimensions, materials, and target electrical properties. The overall dimensions of the abdominal phantom were 100 × 100 × 100 mm3, and the thicknesses of the skin, fat, and muscle layers were 2, 6, and 92 mm, respectively. These dimensions were optimized based on the average shape of Japanese male and female adults [33]. To mimic the electrical properties of biological tissues [34], the phantom was constructed using conductive silicone rubber for the skin layer; soybean oil and hydroxystearic acid for the fat layer; and deionized water, sodium chloride, and agar for the muscle layer [35].

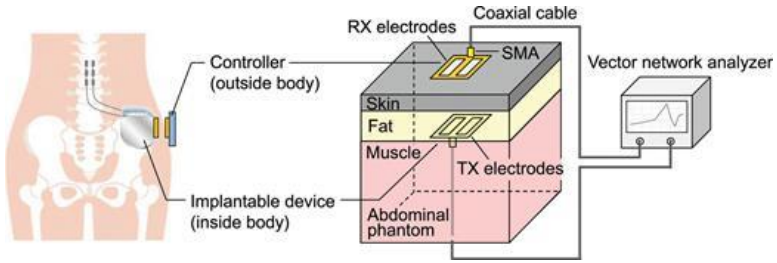

Figure 1: Proposed implantable HBC system and its corresponding measurement setup.

Table 1: Information of the abdominal phantom.

Layer	Dimensions (mm^3)	Materials	Target Electrical Properties
Skin	100 × 100 × 2	Conductive silicone rubber	Conductivity and permittivity of each biological tissue in Gabriel's database[34]
Fat	100 × 100 × 6	Soybean oil	
		Hydroxystearic	
Muscle	100 × 100 × 92	Deionized water	
		Sodium chloride	
		Agar	

Implantable HBC electrodes (Figure. 2) were used as the TX and RX electrodes. A two-electrode structure, commonly used in wearable HBC devices, comprising rolled copper and gold plating on a polyimide substrate of 8 × 24 mm2 was employed. The TX electrodes, implanted at a depth of 8 mm, were placed in contact with the lower part of the fat layer, whereas the RX electrodes were placed on the skin layer surface. As the neurostimulators (48 × 48 × 10 mm3) [36] were fixed to the fascia within 20 mm of the skin surface, the TX electrodes were mounted on a vinyl chloride chassis and placed inside the muscle phantom. The TX and RX electrodes were connected to a vector network analyzer (VNA) (E5080A, Keysight, CA, USA) using coaxial cables, and the transmission characteristics $|S21|$ inside and outside the body were measured at 1–100 MHz. The VNA was operated using utility power. Figure 3 shows a cross section of the abdominal phantom with the RX electrodes and the implanted coaxial cables.

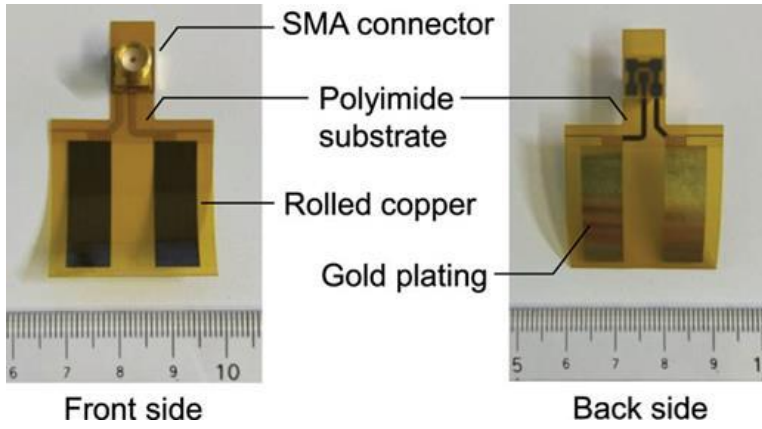

Figure 2: Implantable HBC electrodes used as TX and RX electrodes.

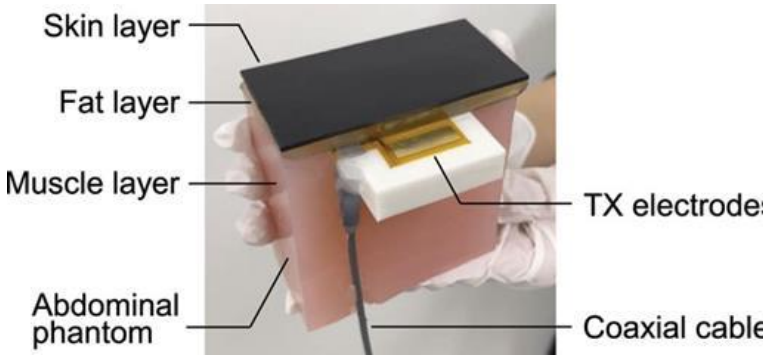

Figure 3: Cross section of the abdominal phantom.

Results and Discussion

Transmission characteristics and its distance-dependent attenuation

Figure 4 shows the measured transmission characteristics |*S*21|, as a function of frequency. The measurements revealed that the maximum |*S*21| was −23.5 dB at 37.2 MHz. The |*S*21| obtained in previous studies focusing on wireless communication in implantable environments similar to this study is shown in Table 2 [2–4,37–41]. The proposed implantable HBC achieved higher transmission characteristics than conventional wireless communication using radio-frequency electromagnetic fields

(RFEMFs) [2,3,37–41] because in the latter, signals are attenuated in biological tissues and transmission characteristics deteriorate. In implantable HBC using carrier frequencies of several tens of MHz, the TX and RX electrodes closely positioned through the skin and fat layers have superior transmission characteristics owing to their strong capacitive coupling. To validate the experimental results, an electromagnetic field simulation employing the finite-difference time-domain method was conducted using a numerical phantom model with the same structure as the phantom used in the measurements. As a result, the simulated $|S_{21}|$ value at 37.2 MHz was −21.8 dB, which closely matched the experimental value of −23.5 dB. The proposed electrode structure does not have sharp resonance characteristics such as typical antennas, so we consider that the impact of the electrodes' dimensions on the optimal carrier frequency is minor.

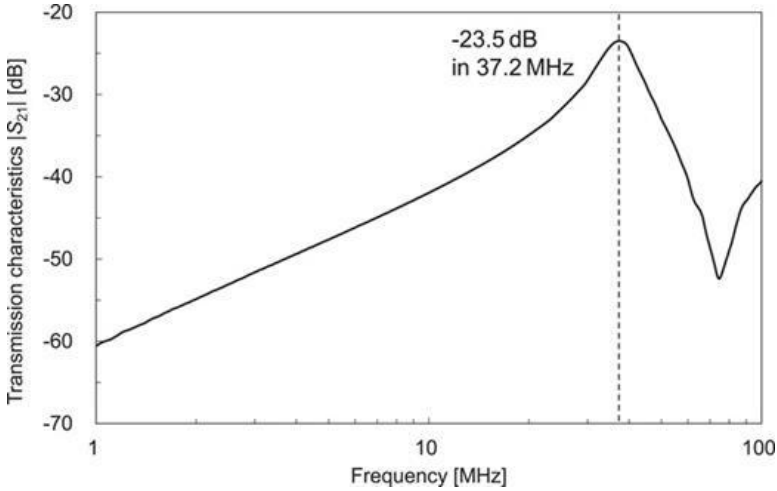

Figure 4: Transmission characteristics $|S_{21}|$ as a function of frequency.

Table 2: Comparison of the proposed implantable HBC and communication systems in similar environments.

References, Year	App.	Method	Study Type	Frequency	Implanted Depth (mm)	S_{21} (dB)
This study	NS[a]	HBC	Exp.	37 MHz	8	−23.5
37, 2015	ND[b]	RFEMF	Exp.	1–6 GHz	50	<−25
					90	<−38
38, 2018	LM[c]	RFEMF	Exp.	4.5–6.5 GHz	45–91.8	<−47
39, 2019	NS[a]	RFEMF	Exp.	403 MHz	10	−51.8
40, 2019	ND[b]	RFEMF	Exp.	22.8 MHz	50	−34.55
				45.6 MHz		−50.16
2, 2021	CE[d]	RFEMF	Sim.	915 MHz	40	−41
				2.25 GHz		−35
				3.1 GHz		−36
				5.8 GHz		−47
				915 MHz	130	−62
				2.25 GHz		−82
				3.1 GHz		−90
				5.8 GHz		−117
3, 2022	CE[d]	RFEMF	Exp.	47 MHz	20	−27.5
				49 MHz		−28
41, 2022	ND[b]	RFEMF	Sim.	400 MHz	50	−28
				900 MHz		−26
				2.4 GHz		−50
			Exp.	21 MHz	50	−30
				400 MHz		−41
		HBC	Sim.	21 MHz	50	−37
4, 2021	CE	HBC	Sim.	3 MHz	20	−38
			Exp.	3 MHz	10	−27
					30	−42

[a] NS Neurostimulator. [b] ND Not defined. [c] LM Liver monitoring. [d] CE Capsule endoscope.

The proposed implantable HBC was evaluated based on its EMI with other electrical devices and its security against unauthorized wireless access from a distance. Figure 5 shows $|S_{21}|$, as a function of the distance between the RX electrodes and skin surface z at 37.2 MHz. Compared with that when the RX electrodes were in contact with the skin (z = 0 mm), $|S_{21}|$ rapidly attenuated by 16.6 dB when the electrodes were 1 mm away from the skin surface because the quasi-static field rapidly deteriorated, which mainly contributes to transmission in implantable HBC, with distance. Thus, the proposed method minimizes the EMI with surrounding devices, demonstrating its effectiveness in terms of electromagnetic compatibility. In addition, the implantable HBC is expected to provide secure communication, thereby protecting against unauthorized wireless access by attackers from a distance.

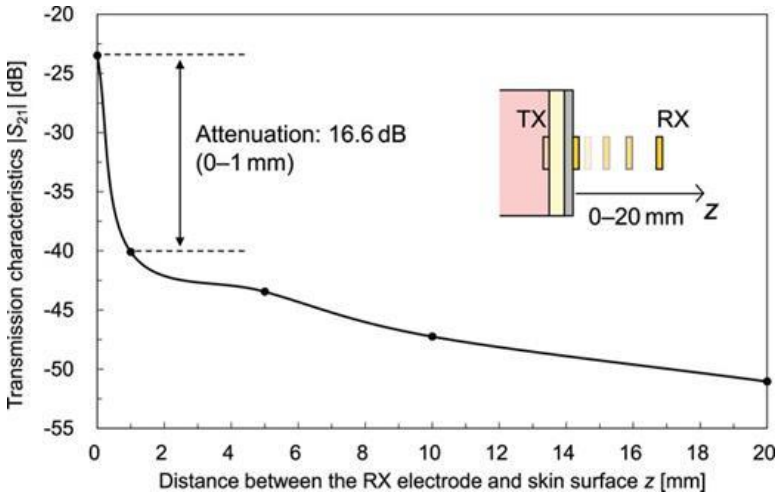

Figure 5: Transmission characteristics $|S_{21}|$ as a function of distance between the RX electrodes and skin surface z.

Optimization of Carrier Frequency Based on Transmission Efficiency–EMI Trade-Off

To optimize the optimal carrier frequency for implantable HBC based on the trade-off between the transmission efficiency and EMI robustness, the evaluation index (*EI*) was defined as follows:

EI=α·GC−(1−α)·GNC, where G_C is $|S_{21}|$ when the RX electrodes are in contact with the skin (z = 0 mm) and G_{NC} is $|S_{21}|$ when the RX electrodes are not in contact with the skin (z = 10 mm), as shown in Figure. 6. Thus, *EI* can assess the performance of implantable HBC based on G_C, which indicates the transmission of the desired signal, and G_{NC}, which represents the interference from undesired signals. The weight of these factors is controlled by the parameter α. If α = 1, only the transmission efficiency is considered; if α = 0, only the EMI is considered. The data rate required for communication between the neurostimulator and the control device is at most a few tens of kbps, and the frequency bandwidth can be considered narrowband. Therefore, the proposed *EI* provides the optimal center carrier frequency. For applications demanding higher data rates, such as the transmission of high-definition images from capsule endoscopes, *EI* definition should be extended to include a bandwidth criterion. The normalized *EI* as a function of frequency for each α is also shown in Figure 6. For example, when α = 0.5, the transmission efficiency and EMI are balanced and the frequency-maximizing *EI* is 36.5 MHz. In contrast, when α is set to 0.25 to prioritize interference suppression, the *EI* increases at lower frequencies. This trend can be attributed to the reduction in G_{NC}, which reflects a decrease in the reception of undesired signals at these frequencies. The *EI* can be used to optimize a carrier frequency that satisfies the requirements of efficiency and EMI for an implantable application while still balancing them.

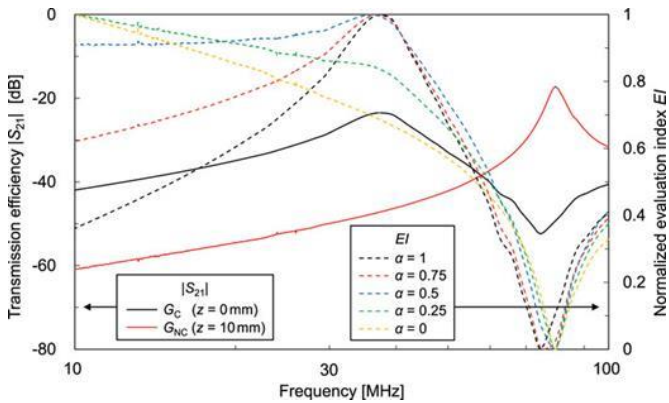

Figure 6: Transmission efficiency $|S_{21}|$ and *EI* as a function of frequency.

Conclusion

Herein, implantable HBC was investigated, particularly for the communication between neural stimulators implanted in the abdomen and a control device outside the body. The transmission characteristics between the inside and outside layers of the abdominal phantom were tested at 1–100 MHz. The implantable HBC achieved a maximum value of −23.5 dB at 37.2 MHz. Furthermore, due to the rapid degradation of transmission characteristics when removing the RX electrodes from the body, the signal from the implanted TX electrodes rarely caused EMI and was robust against unauthorized wireless access from a distance. In addition, the *EI* that considered both the direct contact and non-contact transmission scenarios was introduced. This index effectively guided the selection of an optimal carrier frequency that harmonized transmission efficiency with EMI robustness. The optimization of *EI* highlights the effectiveness of the proposed method in optimizing implantable HBC as well as addressing the technical performance issues, EMI, and information security. These findings offer a foundation for the future development of implantable medical devices, emphasizing the critical balance between operational efficiency and mitigating potential EMI issues. In future work, we will evaluate the influence of device implant positions and surrounding tissue structures on the transmission characteristics of implantable HBC, assuming neurostimulators and other medical devices. In addition, we will investigate the electrode structure that maximizes transmission efficiency.

References

1. F Faisal, M Zada, H Yoo, IB Mabrouk, M Chaker, et al. An ultra-miniaturized antenna with ultra-wide bandwidth for future cardiac leadless pacemaker, IEEE Trans. Antennas Propag. 2022; 70: 5923–5928.
2. M Särestöniemi, C Pomalaza-Raez, K Sayrafian, J Iinatti. IEEE International Conference on Communications Workshops (ICC Workshops) (IEEE, 2021). 2021; 1–5.
3. Y Fujii, H Takagi, J Wang, Y Yokoyama, K Saito, et al. Development of a high-speed implant communication module

deep into the human body: Realized in the 10–60-MHz band with small anten- nas [bioelectromagnetics]. IEEE Antennas Propag. Mag. 2022; 64: 112–125.
4. R Noormohammadi, A Khaleghi, I Balasingham. Galvanic impulse wire- less communication for biomedical implants. IEEE Access. 2021; 9: 38602–38610.
5. BV Medtronic. PillCamTM Capsule Endoscopy User Manual. 2016.
6. MK Aktas, W Zareba, J Butler, A Younis, S McNitt, et al. Confirm Rx insertable cardiac monitor for primary atrial fibrillation detection in high-risk heart failure patients (confirm-AF trial). Ann. Noninvasive Electrocardiol. 2023; 28: 13021.
7. A Iqbal, M Al-Hasan, IB Mabrouk, TA Denidni. Wireless powering and telemetry of deep-body ingestible bioelectronic capsule. IEEE Trans. Antennas Propag. 2022; 70: 9819–9830.
8. ÖF Çelik, SC Ba¸saran. Compact triple-band implantable antenna for multitasking medical devices. J. Electr. Eng. 2022; 73: 166–173.
9. MA Jensen, Y Rahmat-Samii. EM interaction of handset antennas and a human in personal communications. Proc. IEEE. 1995; 83: 7–17.
10. Y Chan, MQH Meng, KL Wu, X Wang. IEEE Engineering in Medicine and Biology 27th Annual Conference (IEEE, 2005), 2005; 7754–7757.
11. A Alomainy, Y Hao. Modeling and characterization of biotelemetric radio channel from ingested implants considering organ contents. IEEE Trans. Antennas Propag. 2009; 57: 999–1005.
12. A Mauludiyanto, G Hendrantoro, MF Nova. The attenuation charac- teristics of the body tissue on frequency function in WBAN channel. JAREE. 2021; 5: 107–113.
13. S Benaissa, L Verloock, D Nikolayev, M Deruyck, G Vermeeren, et al. Propagation-loss char- acterization for livestock implantables at (433, 868, 1400) MHz. IEEE Trans. Antennas Propag. 2021; 69: 5166–5170.
14. MJ Christoe, J Yuan, A Michael, K Kalantar-Zadeh. Bluetooth sig- nal attenuation analysis in human body tissue analogues. IEEE Access. 2021; 9: 85144–85150.
15. American National Standards Institute. American National

Standard recom- mended practice for an on-site, ad hoc test method for estimating electromagnetic immunity of medical devices to radiated radio-frequency (RF) emissions from RF transmitters. in ANSI C63.18-2014 (Revision of ANSI C63.18-1997). 2014; 1–64.

16. V Buzduga, D Witters, J Casamento, W Kainz. Testing the immunity of active implantable medical devices to CW magnetic fields up to 1 MHz by an immersion method. IEEE Trans. Biomed. Eng. 2007; 54: 1679–1686.
17. T Toyoshima. IEEE MTT-S International Microwave Workshop Series on Innovative Wireless Power Transmission: Technologies, Systems, and Applications. 2011; 101–104.
18. MS Darweesh, T Ismail, H Mostafa. 11th International Symposium on Communication Systems, Networks and Digital Signal Processing (CSNDSP) (IEEE, 2018). 2018; 1–6.
19. YC Yalcin, C Kooij, DAMJ Theuns, AA Constantinescu, JJ Brugts, et al. Emerging electromagnetic interferences between implantable cardioverter-defibrillators and left ventricular assist devices. EP Europace. 2020; 22: 584–587.
20. T Nishikawa, T Hikage, M Yamamoto. IEEE International Workshop on Electromagnetics: Applications and Student Innovation Competition (iWEM) (IEEE, 2022). 2018; 124–125.
21. E Kwarteng, M Cebe. A survey on security issues in modern Implantable Devices: Solutions and future issues. Smart Health. 2022; 25: 100-295.
22. A Longras, H Oliveira, S Paiva. 15th Iberian Conference on Information Systems and Technologies (CISTI) (IEEE, 2020). 2020; 1–4.
23. D Zaldivar, LA Tawalbeh, F Muheidat. 10th Annual Computing and Communication Workshop and Conference (CCWC) (IEEE, 2020). 2020; 0488–0493.
24. S Das, GP Siroky, S Lee, D Mehta, R Suri. Cybersecurity: The need for data and patient safety with cardiac implantable electronic devices. Heart Rhythm. 2021; 18: 473–481.
25. R Somasundaram, M Thirugnanam. Review of security challenges in healthcare internet of things. Wireless Network. 2021; 27: 5503–5509.
26. D Muramatsu, M Kodama. Signal transmission analysis in

implantable human body communication for abdominal medical devices. AIP Adv. 2023; 13: 085022.
27. D Das, S Maity, B Chatterjee, S Sen, Enabling covert body area net- work using electro-quasistatic human body communication. Sci. Rep. 2019; 9: 41-60.
28. International Telecommunication Union, Radio Regulations, Edition of 2020 (ITU, 2020), Vol. 1.
29. IEEE Standards Association. IEEE Standard for Local and metropolitan area networks—Part 15.6: Wireless Body Area Networks. 2012.
30. D Muramatsu, K Sasaki. Transmission analysis in human body com- munication for head-mounted wearable devices. Electronics. 2021; 10: 12-13.
31. MN Islam, MR Yuce. Review of medical implant communication system (MICS) band and network. ICT Express. 2016; 2: 188–194.
32. C Han, J Mao, X Wang, S Yu, Z Zhang. IEEE International Symposium on Circuits and Systems (ISCAS) (IEEE, 2021). 2021; 1–5.
33. WF W Southwood. The thickness of the skin. Plast. Reconstr. Surg. 1955; 15: 423–429.
34. S Gabriel, RW Lau, C Gabriel. Phys. Med. Biol. 1996; 41: 22-51.
35. D Muramatsu, F Koshiji, K Koshiji, K Sasaki. Development and study of electrical property on phantom for human body communication consider- ing tissue structure of human arm. J. Jpn. Inst. Electron. Packag. 2014; 17: 63–68.
36. St. Jude Medical, Proclaim Implantable Pulse Generator Clinician's Manual. 2017.
37. PA Floor, R Chavez-Santiago, S Brovoll, O Aardal, J Bergsland, et al. In-body to on-body ultrawideband propagation model derived from measurements in living animals. IEEE J. Biomed. Health Inf. 2015; 19: 938–948.
38. P Leelatien, K Ito, K Saito, M Sharma, A Alomainy. Channel character- istics and wireless telemetry performance of transplanted organ monitoring sys- tem using ultrawideband communication. IEEE J. Electromagn. RF Microwaves Med. Biol. 2018; 2: 94–101.
39. Y Feng, Y Li, L Li, B Ma, H Hao, et al. Tissue-dependent Co-matching method for dual-mode antenna in implantable

neurostimulators," IEEE Trans. Antennas Propag. 2019; 67: 5253–5264.
40. H Liu, J Shi, S Wu, X Wang, J Wang. International Workshop on Electromagnetics: Applications and Student Innovation Competition (iWEM) (IEEE, 2019), 2019; 1–2.
41. A Datta, M Nath, B Chatterjee, S Maity, S Sen. A quantitative anal- ysis of physical security and path loss with frequency for IBOB channel," IEEE Microwave Wireless Compon. Lett. 2022; 32: 792–795.